Eur. Phys. J. A **29**, 183–188 (2006)
DOI 10.1140/epja/i2006-10077-9

THE EUROPEAN PHYSICAL JOURNAL A

Gamow-Teller beta decay of ^{105}Sn

M. Kavatsyuk[1,2,a], L. Batist[3,4], F. Becker[1], A. Blazhev[1,5], W. Brüchle[1], J. Döring[1], T. Faestermann[6], M. Górska[1], H. Grawe[1], Z. Janas[7], A. Jungclaus[8], M. Karny[7], O. Kavatsyuk[1,2], R. Kirchner[1], M. La Commara[4], S. Mandal[1], C. Mazzocchi[1], I. Mukha[1,9], S. Muralithar[1,10], C. Plettner[1], A. Płochocki[7], E. Roeckl[1], M. Romoli[4], M. Schädel[1], and J. Żylicz[7]

[1] GSI, Darmstadt, Germany
[2] National Taras Shevchenko University of Kyiv, Ukraine
[3] St. Petersburg Nuclear Physics Institute, Russia
[4] Università "Federico II" and INFN, Napoli, Italy
[5] University of Sofia, Bulgaria
[6] Technische Universität München, Germany
[7] University of Warsaw, Poland
[8] Departamento de Fisica Teórica, Universidad Autonoma de Madrid, Spain
[9] Kurchatov Institute, Moscow, Russia
[10] Nuclear Science Center, New Delhi, India

Received: 16 May 2006 / Revised: 27 July 2006 /
Published online: 29 August 2006 –
Communicated by J. Äystö

Abstract. The β-decay of ^{105}Sn was re-investigated at the ISOL facility of GSI Darmstadt by using a total absorption spectrometer. The experimental results include the half-life and β-delayed proton branching ratio of 32.7(5) s and $1.1(4) \cdot 10^{-4}$, respectively, and the contribution of electron capture to the ^{105}Sn decay of 0.420(35). The Gamow-Teller strength distribution peaking at 3.6 MeV was measured, yielding a summed Gamow-Teller strength of 3.0(4). The latter data are discussed in comparison with shell-model predictions based on an empirical interaction.

PACS. 27.60.+j $90 \leq A \leq 149$ – 23.40.-s Beta decay; double beta decay; electron and muon capture – 21.10.Tg Lifetimes – 21.60.Cs Shell model

1 Introduction

The interest in studying nuclei in the ^{100}Sn region, in particular those "south-east" of this doubly magic shell closure, is partly motivated by the occurrence of a resonance-like β decay related to the Gamow-Teller (GT) transitions of a $\pi g_{9/2}$ proton into a $\nu g_{7/2}$ neutron. For odd-A tin isotopes, this transformation proceeds within the even-even core, leading to three-quasiparticle states in the odd-Z, even-N daughter nucleus and a correspondingly complex structure of the GT resonance. A suitable tool for measuring the β-intensity distribution in such cases is the total absorption spectroscopy. This method is based on recording cascades of β-delayed γ-rays rather than single γ transitions. This allows one to determine the entire β-intensity distribution, including weak β transitions to high-lying excited states in the daughter nucleus.

The experimental data described here were obtained by means of the total absorption spectrometer (TAS) at the ISOL facility of GSI Darmstadt [1]. This work is part of a research program on nuclei near ^{100}Sn performed at this facility, including in particular recent investigations of ^{94}Rh [2], ^{94}Pd [2], ^{94}Ag [3–6], ^{97}Ag [7], ^{98}Ag [8], ^{100}In [9], ^{102}In [10], ^{101}Sn [11], ^{102}Sn [12], ^{103}Sn [13] and ^{104}Sn [12]. The motivation for the present study of ^{105}Sn was to improve the data available for this decay, with the aim of determining the GT strength distribution and comparing it with shell-model predictions. The results from previous experiments concern, in particular, the β-delayed γ [14] and proton (βp) [15] emission of ^{105}Sn. By using part of the data presented in this work, the Q_{EC} value of this nucleus has been determined to be 6230(80) keV [16]. The β decay of ^{105}Sn is sketched in fig. 1 including the GT strength obtained in this work.

2 Experimental technique

^{105}Sn was produced in a fusion-evaporation reaction, namely ^{50}Cr(^{58}Ni, 2p1n)^{105}Sn. A 5.2 MeV/u ^{58}Ni beam

[a] e-mail: M.Kavatsyuk@gsi.de

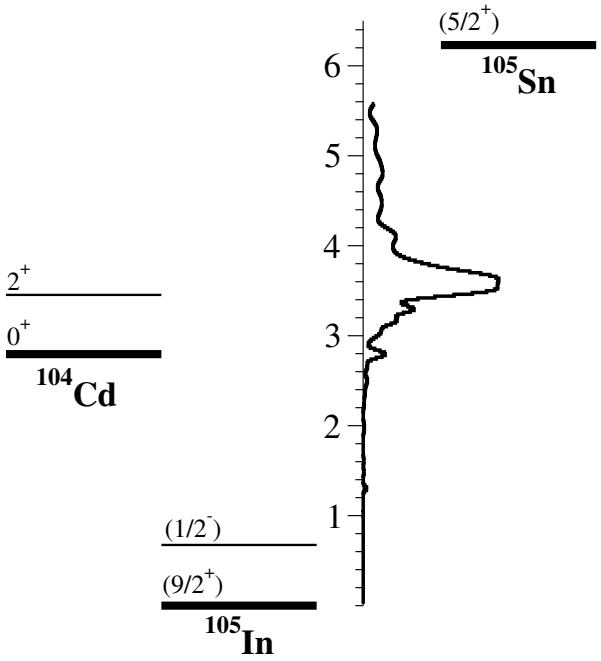

Fig. 1. Simplified decay scheme of ^{105}Sn showing the ground state and the first excited state of the β-decay daughter ^{105}In and the β-delayed proton daughter ^{104}Cd together with the β-strength function of the ^{105}Sn decay (see text).

with an intensity of about 40 particle-nA impinged on enriched ^{50}Cr targets (3–4 mg/cm^2, enrichment 97%). A FEBIAD-B3C ion source with a ZrO_2 catcher was used to extract radioactive species. A high chemical selectivity for the tin was achieved by adding CS_2 vapour to the ion source. Using this technique about 60% of the tin ion-output is shifted to the SnS^+ molecular side-band, thus suppressing strongly the In, Cd, Ag, and Pd isobaric contaminants [17]. After ionisation, acceleration to 55 keV and mass separation in a magnetic sector field, the $A = 105 + 32$ ions were implanted into a transport tape, with the resulting radioactive sources being regularly moved to the centre of the TAS. In order to reduce the probability of registering pileup events in the TAS, the intensity of the $A = 105 + 32$ beam, whose dominant component consisted of ^{105}Sn, was deliberately kept at about 1300 atoms/s by choosing a lower than optimum ^{58}Ni energy and introducing slits on the mass-separated beam. Each implantation measurement cycle consisted of consecutive time intervals of 32, 0.8 and 64 s used for implantation, transport and measurement, respectively. The measurement of the ^{105}Sn sources was performed simultaneously with the implantation of the subsequent sources. The total number of such cycles was 465, corresponding to a total measuring time of 8.5 h. In order to obtain pure ^{105}Sn data, the ^{105}In and ^{105}Cd contributions to the $A = 105 + 32$ measurement were determined in separate experiments with 32, 0.8, 256 and 64, 0.8, 256 s cycles, accumulating 48 and 28 such sources, respectively.

The TAS [18] consists of a large NaI crystal. In the following the pulse-height distribution obtained from this crystal is called "TAS spectrum". The TAS includes ancillary detectors, namely a planar Ge X-ray (GEX) and two silicon (TOP and BOT) charged-particle detectors. The GEX detector was used to select the electron capture (EC) decay of interest by registering characteristic $K_{\alpha,\beta}$ X-rays. By demanding coincidence with signals from the silicon detectors, the β^+ component of the decay was selected. The BOT detector, viewing the transport tape from the side of the ion implantation, was used to detect positrons as well as β-delayed protons. By means of a Monte Carlo simulation, the proton detection efficiency of the BOT detector was found to be 48^{+2}_{-10}%, which is relevant to the βp studies described in sect. 3.3. For the measurement of a conversion coefficient (see sect. 3.5), the efficiencies of the GEX detector for γ-rays and the TOP and BOT detectors for electrons were measured by using the 661 keV transition in ^{137}Ba, populated in the β decay of a ^{137}Cs source. The spectra accumulated by means of the GEX, TOP and BOT detectors during the $A = 105 + 32$ measurement as well as the gate conditions used for generating the coincident TAS spectra are described in ref. [16].

3 Experimental results

3.1 Experimental TAS spectra

As the singles TAS spectrum is dominated by contributions from the room background, ^{105}Sn decay events were selected by using the ancillary detectors. By demanding coincidence between the TAS signal and the characteristic In X-ray measured by the GEX detector, the EC component of the ^{105}Sn decay was selected (TAS(EC) spectrum). The TAS(EC) spectrum does not suffer from isobaric contamination because of the high resolution of the GEX detector.

As in case of ^{103}Sn decay [13], the exponential tail of low-energy events registered in the TOP and BOT detectors is assigned to positrons while the structure above about 2 MeV is interpreted as being due to βp emission (see sect. 3.3). The energy range between 0.2 and 1.8 MeV was used as a positron condition for both Si detectors. Events observed in the BOT detector, which have energy deposits larger than 1.8 MeV, were considered to mainly stem from protons but include contributions from positrons. By demanding coincidence of the TAS signal with signals from the TOP or/and BOT detector within the positron gate, the β^+ component of the decay was obtained (TAS(β^+)). On the basis of the additional measurements with longer tape cycles (see sect. 2), the ^{105}In and ^{105}Cd contributions were determined and subtracted from the total TAS(β^+) spectrum obtained for $A = 105 + 32$. The subtraction coefficients were deduced by using the X-ray spectra measured by the GEX detector (see ref. [13] for details). All in all, it was found that the total TAS(β^+) spectrum contained a fraction of 14% due to contributions of isobaric contaminants which are mainly due to the decay of the ^{105}In sample on the tape. The resulting TAS(EC) and (background-free) TAS(β^+) spectra are presented in ref. [16].

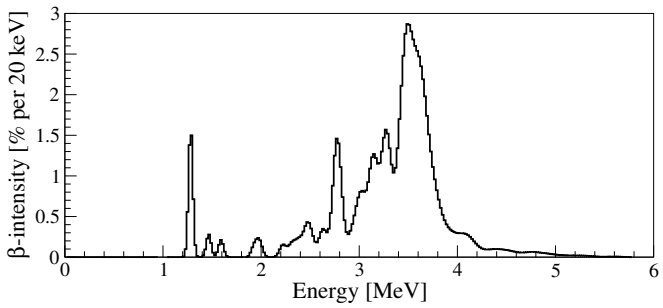

Fig. 2. Beta-intensity distribution for the ^{105}Sn decay obtained by de-convoluting the TAS(EC) and TAS(β^+) spectra.

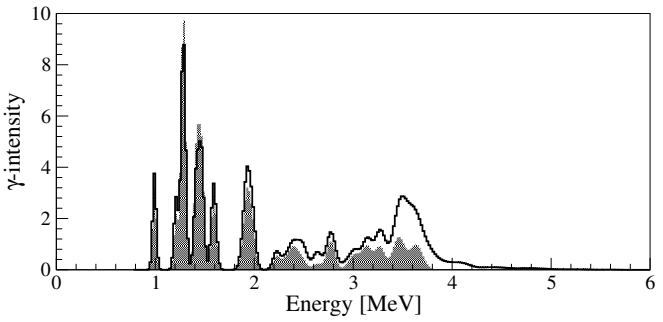

Fig. 3. Intensities of β-delayed γ-rays from the ^{105}Sn decay as a function of the ^{105}In excitation energy. The γ intensity is defined as the number of quanta emitted per 100 decays, integrated over an excitation energy interval of 20 keV. The TAS results (black-line histogram) are compared to data obtained in ref. [14] (shaded-area histogram). The latter distribution has been folded with the TAS resolution.

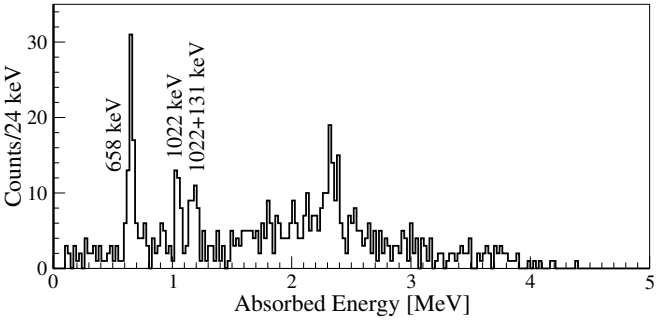

Fig. 4. TAS spectrum gated by β-delayed protons from the ^{105}Sn decay.

The efficiencies of the gate conditions set on the Si and GEX signals were deduced from the decomposition of the singles TAS spectrum into EC and β^+ components. This procedure was chosen as the TAS(β^+) and TAS(EC) spectra have lower statistics than the singles TAS spectrum. The values resulting for the efficiency of the gate conditions chosen to obtain the TAS(β^+) and TAS(EC) amounted to 88(1)% and 6.6(5)%, respectively. These values agree with those obtained by using ^{103,106}Sn data [13]. For more details on the evaluation of the TAS gate efficiencies, see ref. [13]. Combining the measured efficiency values with the number of counts in the TAS(β^+) and TAS(EC) spectra an EC contribution of 0.420(35) was obtained for the ^{105}Sn decay. The latter value was used to determine the Q_{EC} of this nucleus [16].

3.2 Beta-intensity distribution

The method described in ref. [13] was used to determine the β-intensity distribution for ^{105}Sn. The level scheme obtained from the high-resolution measurement [14] was taken as an input for the simulation of the TAS response function, required for the de-convolution procedure. However, due to the low efficiency of the high-resolution setup weak β-delayed γ transitions have remained unobserved. Correspondingly, the decay scheme obtained in ref. [14] is incomplete, and hence assumptions have to be made in deducing β intensities. For this purpose, the range of ^{105}In excitation energy above 2.8 MeV was divided into energy intervals of 50 keV which were treated as "single levels" populated in β decay.

The final β-intensity distribution is shown in fig. 2. To verify the de-convolution procedure, the intensity distribution (I_γ) of β-delayed γ-rays as a function of ^{105}In excitation energy was calculated after each fitting step. The comparison of the resulting I_γ spectrum with that obtained from the high-resolution data [14], is shown in fig. 3. The two distributions agree below 2.5 MeV which proves that the high-resolution data and those obtained by unfolding the TAS spectra are consistent for low ^{105}In excitation energies. However, above 2.5 MeV the TAS measurement yields higher γ-ray intensities, indicating the existence of close-lying and weakly populated levels that escaped identification with the germanium array used in ref. [14].

3.3 Beta-delayed proton emission

The TAS serves to identify the final states populated in βp decay by detecting γ-rays following proton emission. Moreover, the total absorption effect in the TAS offers the chance of discriminating between the EC and β^+ decay modes.

Figure 4 displays the TAS spectrum measured in coincidence with βp decay of ^{105}Sn, events of the latter type being registered in the BOT detector. The 658 keV peak corresponds to the βp decay to the first excited state in ^{104}Cd after EC (ECp) decay. The 1022 keV peak stems from proton transitions to the ^{104}Cd ground state after positron (β^+p) decay of ^{105}Sn. The ECp decay to the ground state of the ^{104}Cd is characterised by the absence of TAS signals. The corresponding proton spectrum measured by the BOT detector in anti-coincidence with TAS signals is shown in the lower panel of fig. 5. The structure observed in the spectrum of the BOT detector, for absorbed energies below 1.5 MeV is related to the detection of conversion electrons emitted in the decay of the $1/2^-$ isomer of ^{105}In (see sect. 3.5).

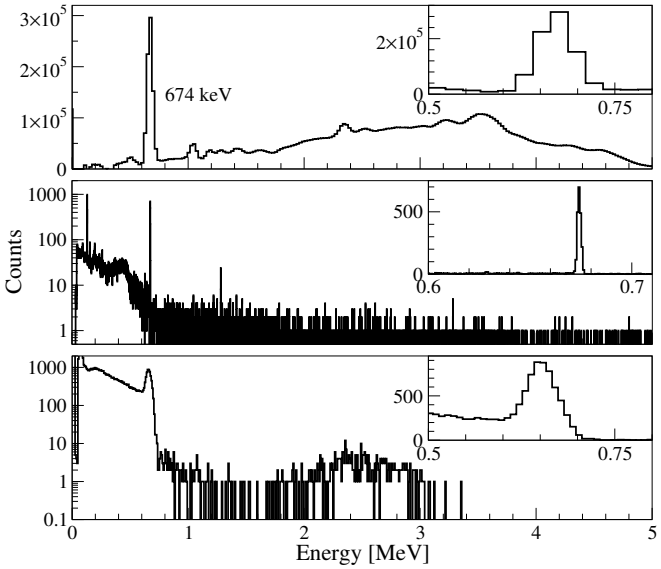

Fig. 5. Background-free singles TAS spectrum (upper panel) obtained for $A = 105 + 32$. Gamma-ray (middle panel) and charged-particle (lower panel) spectra were obtained by using the GEX and BOT detectors, respectively, in anti-coincidence with the TAS. The insets show the γ-ray and conversion-electron lines assigned to the de-excitation of the 674 keV, $1/2^-$ isomer in ^{105}In.

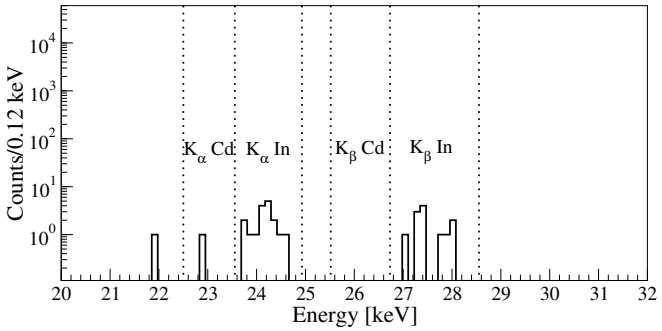

Fig. 6. Singles X-ray spectrum (grey-line histogram) and proton-gated X-ray spectrum measured by the GEX detector in anti-coincidence with TAS (full-line histogram), obtained for the $A = 105 + 32$ measurement.

The $1022 + 131$ keV peak occurring in the βp-gated TAS spectrum indicates the population of the 131 keV level of ^{105}Cd in the β^+ decay ^{105}In. In this case, positrons were apparently registered within the proton energy window of the BOT detector. The same seems to hold for the bump of the βp-gated TAS spectrum, that extends from 1.5 to 4 MeV. Moreover, it was impossible to deduce the β-intensity distribution related to the βp decay of ^{105}Sn due to the positron contribution to the proton gate.

The βp-gated TAS spectrum was decomposed into the above-mentioned contributions representing β^+p and ECp transitions to the ground state and first exited state of ^{104}Cd using simulated TAS response functions. This procedure allows to deduce intensities of individual βp decay branches. However, no conclusion could be drawn on the intensity of the β^+p transition to the first excited state in ^{104}Cd, which would correspond to a $1022 + 658$ keV peak in the βp-gated TAS spectrum. The probability of such a process is presumably very low, as was shown for the case of the ^{103}Sn βp-decay [13]. The resulting relative branching ratio of the β^+p transition to the first exited state of ^{102}Cd was estimated to be less than 2%.

By combining the βp intensities with the total number of counts recorded in the TAS(EC) and TAS(β^+) spectra and taking into account the corresponding gate efficiencies, a branching ratio of $11(4) \cdot 10^{-5}$ was found for the βp decay of ^{105}Sn. The partial intensities of ECp and β^+ transitions to the ground state of ^{104}Cd are $8(3) \cdot 10^{-5}$ and $1(1) \cdot 10^{-5}$, respectively, while that of the ECp decay to the first excited state of ^{104}Cd is $2.1(7) \cdot 10^{-5}$. The 1022 keV annihilation peak, that occurs in the βp-gated TAS spectrum and indicates the β^+p transition to the ground state of ^{104}Cd, may contain a contribution due to the registration of positrons in the proton gate. Therefore, the relative branching ratio of $1 \cdot 10^{-5}$ found for this β^+p transition was assumed to have a relative uncertainty of 100%.

Measurement of the proton X-ray coincidences allows one to deduce the mean width of excited states in the β-decay daughter [19,20]. The X-ray spectrum measured by the GEX detector in coincidence with protons registered in the BOT detector is shown in fig. 6. To purify the spectrum from contaminants an additional condition of anti-coincidence with the TAS signal was applied. This condition selects the strongest branch of the ECp decay, namely that to the ^{104}Cd ground state. The intensity ratio $I_{KX}(\mathrm{Cd})/I_{KX}(\mathrm{In})$ was estimated to be $1/29 = 0.03(3)$, where $I_{KX}(\mathrm{Cd})$ and $I_{KX}(\mathrm{In})$ corresponds to the number of K_α plus K_β events registered in the characteristic cadmium and indium X-ray lines, respectively. Using this ratio and the total width of the K-shell vacancy state in a tin atom of 8.53 eV [21], the mean width of excited nuclear states in ^{105}In was determined to be 0.25(25) eV. This value is close to that obtained for ^{103}In [13] and ^{113}I [20].

3.4 Beta-decay half-life

The β-decay half-life of ^{105}Sn was determined by analysing the dependence of TAS events as a function of the time elapsed after the arrival of a fresh source (see sect. 2). The time profiles were fitted by a single-component exponential decay curve using a least-squares method taking into account the dead-time losses of the data acquisition system. The dead time was determined using the rates measured for all incoming and accepted triggers. In order to check the dead-time correction procedure the rate of a precision pulser, uniformly distributed over the measurement, was analysed. This test yielded a systematic uncertainty of 0.4 s for the half-life measurements. The half-life of ^{105}Sn was found to be $32.6 \pm 0.6_{stat} \pm 0.4_{sys}$ s by using events where the energy absorbed in TAS was above 5 MeV and a coinciding signal in the Si detectors was registered. Such a condition selects events related to the ^{105}Sn β^+-decay

Table 1. Experimental data used for determining the conversion coefficient of the 674 keV γ-transition in ^{105}In. The number of events registered in TAS ("TAS") and in the GEX, BOT and TOP detectors, taken in anti-coincidence in the latter three cases ("GEX$\wedge\overline{\text{TAS}}$", "BOT$\wedge\overline{\text{TAS}}$", "TOP$\wedge\overline{\text{TAS}}$") are given together with the corresponding efficiency-corrected values.

Spectrum	Counts	Efficiency-corrected counts
TAS	$730(10)\cdot 10^3$	$1010(140)\cdot 10^3$
GEX $\wedge\ \overline{\text{TAS}}$	2070(50)	$930(130)\cdot 10^3$
BOT $\wedge\ \overline{\text{TAS}}$	12900(300)	$53(3)\cdot 10^3$
TOP $\wedge\ \overline{\text{TAS}}$	10200(250)	$57(8)\cdot 10^3$

as the Q_{EC} value of the daughter nuclei is lower than 5 MeV. Using the time profile of In K_α X-rays a half-life of $32.7 \pm 0.2_{stat} \pm 0.4_{sys}$ s was obtained. The weighted average of the two results yields a half-life of 32.7(5) s for the β decay of ^{105}Sn which is in agreement with, but more accurate than the previously measured value of 34(1) s [14].

3.5 Population of the $1/2^-$ isomer of ^{105}In in the ^{105}Sn β decay

The presence of a long-lived $1/2^-$ isomer in ^{105}In with an excitation energy of 674 keV and a half-life of 48(6) s has been reported in refs. [22] and [23]. As a 674 keV γ-line occurs in the singles TAS spectrum shown in the upper panel of fig. 5, the $1/2^-$ isomer is apparently populated in the β decay of ^{105}Sn. This population presumably proceeds through γ de-excitation of higher-lying ^{105}In levels fed in β decay as a direct β transition from the $5/2^+$ or $7/2^+$ (see sect. 4) to the isomer is forbidden. By demanding anti-coincidence with NaI signals, the 674 keV γ-rays and the corresponding conversion electrons were observed in the spectra taken with the GEX and Si detectors as can be seen from the data displayed in the middle and lower panels of fig. 5, respectively. The intensities observed for the 674 keV peak in the GEX and TAS spectra and for the related conversion electron line in the TOP and BOT spectra are listed in table 1 together with the corresponding efficiency-corrected values. The good agreement between related pairs of efficiency-corrected intensities proves that the respective detector efficiencies (see sect. 2) are correct. Using these data a conversion coefficient of 0.055(6) was obtained for the ^{105}In $1/2^- \rightarrow 9/2^+$ transition in ^{105}In. A comparison of this result with the theoretical value of 0.062 [24] suggests $M4$ polarity of the transition. This confirms the previous multipolarity assignment [23]. A value of 17(2)% was obtained for the above-mentioned, apparently "indirect" feeding of the isomer in ^{105}Sn decay. This result was used during the de-convolution procedure described in sect. 3.2.

4 Discussion

An experimental quantity suited for comparison with theoretical predictions is the β strength function. For an allowed GT transition, the GT strength function ($B(GT)$) can be calculated according to

$$B(GT) = \frac{D \cdot I_\beta(E)}{f(Q_{EC} - E) \cdot T_{1/2}},$$

where $D = 3860(18)$ s denotes the constant corresponding to the value of the axial-vector weak-interaction coupling constant g_A for the decay of the free neutron [25,26], I_β the normalised β intensity, E the excitation energy of the daughter nucleus, and f the statistical rate function. The resulting quantity $B(GT)$ is expressed in units of $g_A^2/4\pi$.

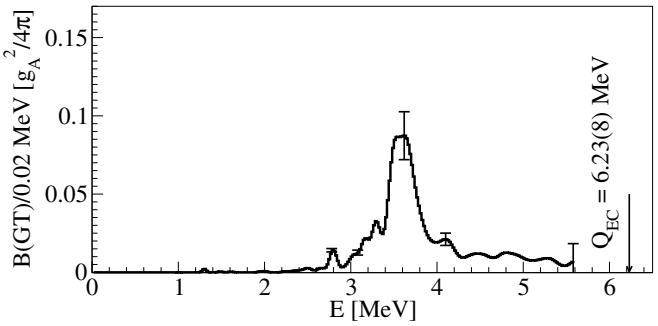

Fig. 7. Gamow-Teller strength distribution for ^{105}Sn obtained from the TAS measurement (black-line histogram) and from the shell-model calculation (dotted histogram). The theoretical distribution was normalised to the summed experimental $B(GT)$ value (see text).

The experimental GT strength, displayed in fig. 7, was calculated using the Q_{EC} value of 6230(80) keV [16], the half-life of 32.7(5) s (see sect. 3.4), and the I_β distribution shown in fig. 2. The summed GT strength $\sum B(GT)$ of ^{105}Sn, deduced from these data, was found to be 3.0(4). The fraction related to βp emission is not included in this value as it was impossible to reliably deduce the βp intensity (see sect. 3.3). However, an estimate based on the βp intensity deduced from the proton spectrum, shown in the lower panel of fig. 5, yielded a $\sum B(GT)$ value of 0.006 for the strongest βp branch, namely the ECp decay to the ^{104}Cd ground state. Therefore, we conclude that the βp branch yields a negligibly small contribution to the $B(GT)$ distribution. The difference between the $\sum B(GT)$ value of ^{105}Sn reported here and the value of 2.9(4) given in a recent conference contribution [27] is due to the fact that in the latter case the β-decay half-life was taken as 34(1) s [14]. Preliminary results have recently been published on the masses of ^{105}Sn and ^{105}In [28]. The corresponding Q_{EC} value of ^{105}Sn is larger only by about 80 keV than the value used in our work.

The resonance-like shape of the experimental GT strength distribution, shown in fig. 7, peaks at an ^{105}In excitation energy of about 3.6 MeV. This decay feature is interpreted as the $\pi g_{9/2} \rightarrow \nu g_{7/2}$ GT transformation occurring within the even-even core and leading to three-quasiparticle states in the odd-Z, even-N daughter nucleus. Figure 7 shows also the theoretical $B(GT)$ distribution obtained from a shell-model calculation by means of the code OXBASH [29] in the $\pi(1g_{9/2}, 2p_{1/2})^{11} - \nu(1g_{7/2}, 2d_{5/2}, 2d_{3/2}, 3s_{1/2}, 1h_{11/2})^6$ model space using the

SNB interaction described in refs. [30,31]. The predicted GT strength distribution displayed in fig. 7 was normalised to the summed experimental GT strength,whereas the predicted $\sum B(GT)$ value is significantly larger than the experimental one. The corresponding "quenching" or "hindrance", expressed as the ratio between theoretical and experimental $\sum B(GT)$ value, amounts to 4.5(6) for ^{105}Sn. Most of the hindrance is believed to be explained by core polarisation and higher-order configuration mixing [32].

Like in case of the ^{103}Sn decay [13], the predicted GT resonance lies lower in excitation energy by about 600 keV compared to the experimental result, as can be seen from fig. 7. This can be partially ascribed to the fact that the SNB interaction predicts the neutron $g_{7/2}$ to be below the $d_{5/2}$ by 50 keV, whereas from an experimental extrapolation [33] the reversed order with a difference of 110(40) keV is inferred, which in total accounts for 160(40) keV of the observed discrepancy. A tuning of the $\pi g_{9/2}$ $\nu(d_{5/2}, g_{7/2})$ monopoles could repair this deficiency, but would be overcompensated by a 10% increase of the $\pi g_{9/2}$ $\nu g_{7/2}$ interaction, that has been proposed to account for the too small width of the GT resonance [7]. It is worth noting that the positions of the GT resonances in the decay of even-N nuclei are well reproduced [7,12] in the shell-model approach of ref. [31]. Therefore a too small neutron-neutron pairing most likely causes the downward shift of the GT resonance in the case of the decay of odd-N parent nuclei such as ^{103,105}Sn.

5 Summary

A re-investigation of the ^{105}Sn β decay was performed by applying the highly selective sulfurisation technique which yielded a highly purified ISOL beam. The TAS allowed to measure the GT strength distribution of this decay for the first time. The decay properties of ^{105}Sn such as half-life, EC contribution and βp branching ratio were determined to be 32.7(5) s, 0.420(35) and $1.1(4) \cdot 10^{-4}$, respectively. Moreover, the TAS was used to measure the population of the $1/2^-$ isomer of ^{105}In in ^{105}Sn decay and to confirm the multipolarity of the isomeric transition.

A dominant GT resonance occurring in the decay of ^{105}Sn was identified, peaking at 3.6 MeV and having a width of 300 keV. A shell-model calculation with an empirical interaction yielded qualitative agreement with the shape of the measured GT resonance. However, the theoretical distribution is shifted by about 600 keV towards lower excitation energies, and the predicted summed GT strength is 4.5(6) times higher than the experimental one. This hindrance is in agreement with the values obtained for other nuclei in the ^{100}Sn region. The total absorption spectroscopy, being complementary to high-resolution studies, thus provides qualitatively new data on the GT strength distribution that are required for testing theoretical models.

The authors would like to thank K. Burkard and W. Hüller for their contribution to the development and operation of the GSI on-line mass separator.

References

1. E. Roeckl *et al.*, Nucl. Instrum. Methods B **204**, 53 (2003).
2. L. Batist *et al.*, Eur. Phys. J. A **29**, 175 (2006) (this issue).
3. C. Plettner *et al.*, Nucl. Phys. A **733**, 20 (2004).
4. I. Mukha *et al.*, Phys. Rev. C **70**, 044311 (2004).
5. I. Mukha *et al.*, Phys. Rev. Lett. **95**, 022501 (2005).
6. I. Mukha *et al.*, Nature **439**, 298 (2006).
7. Z. Hu *et al.*, Phys. Rev. C **60**, 024315 (1999).
8. Z. Hu *et al.*, Phys. Rev. C **62**, 026315 (2000).
9. C. Plettner *et al.*, Phys. Rev. C **66**, 011319 (2002).
10. M. Gierlik *et al.*, Nucl. Phys. A **724**, 313 (2003).
11. O. Kavatsyuk *et al.*, to be published in GSI Sci. Rep. 2006.
12. M. Karny *et al.*, Eur. Phys. J. A **27**, 129 (2006).
13. O. Kavatsyuk *et al.*, Eur. Phys. J. A **25**, 211 (2005).
14. M. Pfützner *et al.*, Nucl. Phys. A **581**, 205 (1995).
15. P. Tidemand-Petersson *et al.*, Z. Phys. A **302**, 343 (1981).
16. M. Kavatsyuk *et al.*, Int. J. Mass Spectrom. **251**, 138 (2006).
17. R. Kirchner, Nucl. Instrum. Methods B **204**, 179 (2003).
18. M. Karny *et al.*, Nucl. Instrum. Methods B **126**, 411 (1997).
19. J.C. Hardy *et al.*, Phys. Rev. Lett. **37**, 133 (1976).
20. Z. Janas *et al.*, Eur. Phys. J. A **23**, 197 (2005).
21. J.L. Campbell, T. Papp, At. Data Nucl. Data Tables **77**, 1 (2001).
22. J. Rivier, R. Moret, Radiochim. Acta **22**, 27 (1975).
23. J. Verplancke *et al.*, Z. Phys. A **315**, 307 (1984).
24. I.M. Band *et al.*, At. Data Nucl. Data Tables **81**, 1 (2002).
25. E. Klempt *et al.*, Z. Phys. C **37**, 179 (1988).
26. S.J. Freedman, Comments Nucl. Part. Phys. **19**, 209 (1990).
27. M. Kavatsyuk *et al.*, Eur. Phys. J. A **25**, s01, 139 (2005).
28. J.A. Clark *et al.*, Eur. Phys. J. A **25**, s01, 629 (2005).
29. B.A. Brown, A. Etchegoyen, W.D.M. Rae, Computer Code OXBASH, MSU-NSCL Report **524** (1988).
30. K. Rykaczewski, GSI-95-09 (1995).
31. B.A. Brown, K. Rykaczewski, Phys. Rev. C **50**, R2270 (1994).
32. I.S. Towner, Nucl. Phys. A **444**, 402 (1985).
33. C. Fahlander *et al.*, Phys. Rev. C **63**, 021307(R) (2001).